

Hydrogen isotope double differential production cross sections induced by 62.7 MeV neutrons on a lead target

M. Kerveno,* F. Haddad, Ph. Eudes, T. Kirchner, and C. Lebrun
SUBATECH, F-44307 Nantes cedex 03, France

I. Slypen and J. P. Meulders
Institut de Physique Nucléaire, 1348 Louvain-la-Neuve, Belgium

C. Le Brun,* F. R. Lecolley, J. F. Lecolley, M. Louvel, and F. Lefèbvres
Laboratoire de Physique Corpusculaire, F-14050 Caen cedex, France

S. Hilaire
Département de Physique Théorique et Appliquée, Service de Physique Nucléaire, B.P. 12 - F-91680 Bruyères-le-Châtel, France

A. J. Koning
Nuclear Research and Consultancy Group, P.O. Box 25, NL-1755 ZG Petten, The Netherlands
 (Received 7 January 2002; published 3 July 2002)

Double differential hydrogen isotope production cross sections have been extracted in 62.7 MeV neutron induced reactions on a lead target. The angular distribution was measured at eight angles from 20° to 160° allowing the extraction of angle-differential, energy differential, and total production cross sections. A first set of comparisons with several theoretical calculations is also presented.

DOI: 10.1103/PhysRevC.66.014601

PACS number(s): 25.40.-h, 27.80.+w, 28.20.-v

I. INTRODUCTION

In recent years, there has been a growing interest in medium energy nucleon induced reactions. Improving our knowledge in this field is important for a number of applications using accelerators such as, for example, cancer therapy or the development of intense neutron sources. Such sources have been considered as possible tools for materials science studies or to tackle the nuclear waste management problem using hybrid systems [1,2].

A hybrid system combines an intense high energy proton beam with a subcritical fission reactor. In this system, 1 GeV protons induce spallation reactions on a heavy target. These reactions produce a large number of neutrons as well as light charged particles (protons, deuterons, ...) over a wide energy range (up to 1 GeV). The neutron source thus created and coupled with a subcritical reactor acts as an additional external source allowing the transmutation of the most toxic nuclear waste (such as minor actinides).

To predict the behavior of such a complex system, it is necessary to make macroscopic simulations which rely on serious basic nuclear reaction data. These data can be obtained directly from experimental results when they exist. This is the case below 20 MeV where databases are available, allowing simulations to provide results with a good level of confidence at least for the U-Pu cycle. They can also be obtained by using theoretical models. As an example, above 150 MeV the intranuclear cascade model, which provides good results [3], is included in the simulation codes.

In the energy region between 20 and 150 MeV, where few experimental results are available, several reaction mechanisms contribute to the production of particles. By studying the energy spectra at different angles, it is possible to better understand the different mechanisms (see Fig. 9). Indeed, the evaporation process, which contributes to the low energy part of the spectra is isotropic in the center of mass of the emitter. On the contrary, direct processes, which correspond to a simple interaction process of the nucleon with the nucleus are characterized by a discrete structure in the spectra. Finally, preequilibrium emission corresponds to much more complex behavior and is strongly focused in the beam direction due to a remaining memory of the incident nucleon direction. These different mechanisms are mixed, implying a quite complex theoretical treatment.

A way to overcome this problem is to base simulations on evaluated data which ensure a good link between low- and high-energy processes [5]. These evaluated data are elaborated using complex preequilibrium models and should reach 200 MeV [5] providing that theoretical codes can have sufficient predictive power in this energy range. Thus it is necessary to measure new cross sections to constrain these codes in order to improve their predictive power.

This work is a part of a large concerted program of nuclear data measurements, HINDAS [6], which is now carried out by several European laboratories to measure double differential production cross sections for neutrons and light charged particles in nucleon induced reactions on different targets (Fe, Pb, and U).

After a description of the neutron beam characteristics, we present the experimental setup in Sec. II. The method of the analysis, calibration and corrections, is described in Sec. III and the double differential cross sections for proton, deu-

*Present address: Institut des Sciences Nucléaire-Grenoble, France.

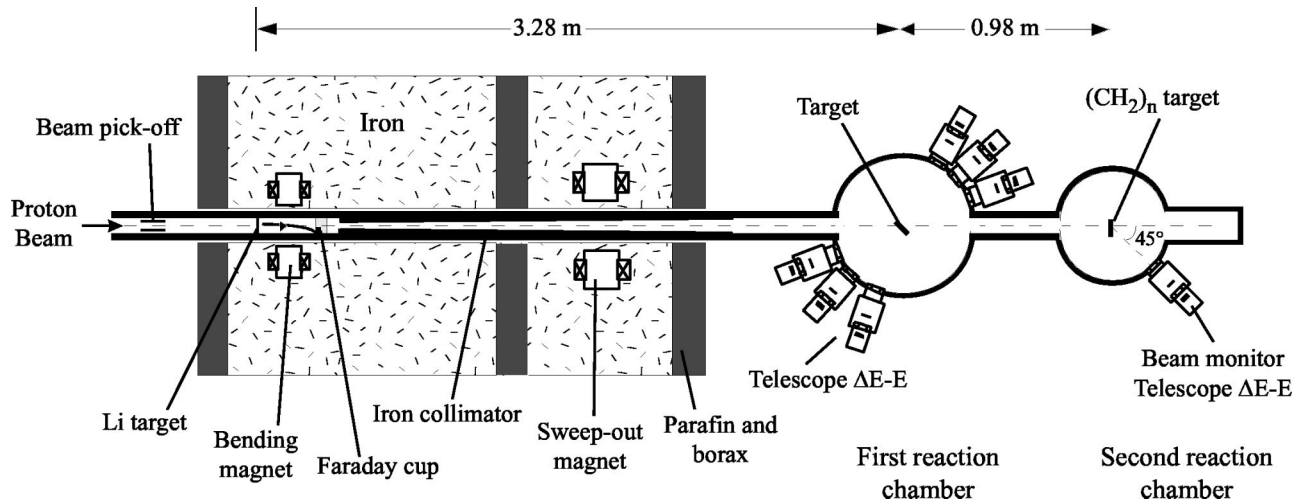


FIG. 1. Global view of the neutron line: neutron production area followed by our experimental setup.

teron, and triton production obtained for 62.7 MeV neutrons on lead are presented in Sec. IV. In Sec. V, the results are compared to well established theoretical code calculations. Finally the conclusions of this work are given in Sec. VI.

II. EXPERIMENTAL SETUP

The experiment was done using the fast neutron facility available at the cyclotron CYCLONE in Louvain-la-Neuve. The neutron beam is obtained via the ${}^7\text{Li}(p,n){}^7\text{Be}_{g.s.}$ ($Q = -1.644$ MeV) and the ${}^7\text{Li}(p,n){}^7\text{Be}^*$ (0.431 MeV) reactions. The layout of the neutron facility (neutron production area and scattering chambers) is shown in Fig. 1 [7,10]. A beam pick off, BPO, is placed upstream from the lithium target in order to get the time at which the neutrons are created. A heavy shielding, made of iron and borated paraffin, surrounds the lithium target and the Faraday cup. This Faraday cup collects the noninteracting protons after deflection by a magnetic field and is used as a beam monitor. After collimation, about 10^6 n/s are available at 0° for a $10\ \mu\text{A}$, 65 MeV proton beam interacting on a 3 mm thick natural lithium target [8].

The scattering chamber is located 3.28 m downstream from the neutron production point and is followed by a second chamber which contains a $(\text{C}_3\text{H}_6)_n$ target and a telescope at 45° . This detector is used as a second beam monitor by counting the protons from the $\text{H}(n,p)$ scattering. During the experiment, the two monitoring systems were in agreement within less than 2%. The characteristics of the neutron beam at the target location are reported in Fig. 2. The neutron energy spectrum shows a well-defined peak which contains about 50% of the neutrons and a flat continuum at low neutron energy. The intensity at the peak maximum is about eight times greater than the intensity of the continuum. For 65 MeV protons, the peak maximum is located at 62.7 MeV and the full width at half maximum is 4 MeV. The radial distribution of the neutron beam normalized to the intensity in the center at the target location is plotted in the inset of Fig. 2. It is found that the neutron beam spot is quite wide, its diameter being almost 4 cm.

The experimental setup of this experiment, based on the one used by the group of Meulders [8,9,11], was improved to allow the use of six telescopes simultaneously. Each telescope is composed of a ΔE detector (100 μm thick and 4 cm in diameter NE102 plastic scintillator) and an E detector [22 mm thick and 38.1 mm in diameter CsI(Tl) crystal]. As shown in Fig. 3, a set of two collimators is used to precisely define the detection solid angle. These collimators are made of copper. The front collimator is a cylinder having an internal diameter of 10 mm, an external diameter of 50 mm and a thickness of 18 mm. The second collimator has an interior diameter of 15 mm, an exterior diameter of 55 mm and a thickness of 18 mm. The ΔE detector gives a fast time signal, which allows the determination of the neutron incident energy by time of flight measurement. The long flight path and the fast time signal ensure a good quality of the reconstructed neutron energy.

The CsI(Tl) thickness has been optimized to stop all the protons, deuterons, tritons and α particles that are produced in this experiment. A pulse shape analysis of the E signal is performed to discriminate between different types of detected particles.

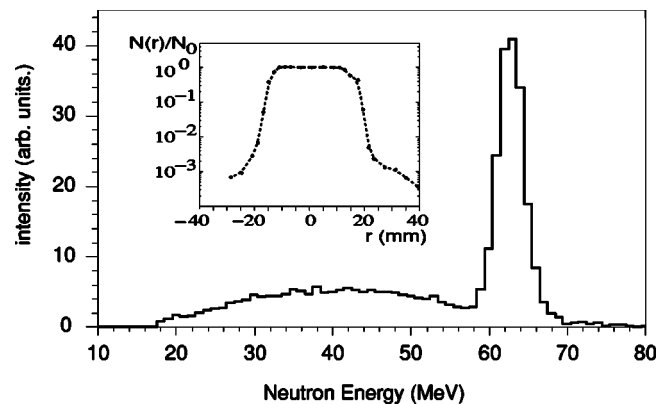


FIG. 2. Neutron energy spectrum deduced from recoil protons on hydrogen for 65 MeV incident proton beam energy on a 3 mm thick Li target. The inset shows the radial neutron intensity normalized to the intensity in the center at target location.

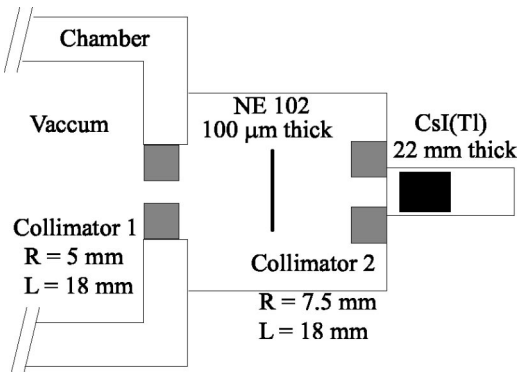


FIG. 3. Schematic view of a telescope.

During the experiment, a quite complete angular distribution has been obtained. Measurements have been performed from 20° to 70° by 10° steps in the forward hemisphere and at 110° and 160° in the backward hemisphere. The low intensity of the neutron beam has compelled us to use a lead target of 0.3 mm. The collection time was then of the order of 60 (120) h for the forward (backward) telescope positions. This ensures the measurement of cross sections as low as $30 \mu\text{b}/\text{sr}/\text{MeV}$ for deuterons with a statistical uncertainty of 10% at backward angles.

III. DATA ANALYSIS

As stated previously, the particle identification is obtained by performing a pulse shape discrimination of the CsI(Tl) detector signal. In addition, most of the background coming from γ or neutron interactions in the crystal is suppressed using $\Delta E - E$ correlation. A clear and easy separation of the different charged particles can then be performed even at low energy as shown in Fig. 4.

A. Calibrations

Since it is not possible to bring charged particle beams in the scattering chamber, calibrations of the detectors have been done using a $(\text{C}_3\text{H}_6)_n$ (1 mm thick) target and a $(\text{CD}_2)_n$ (0.6 mm thick) target. Using these targets, it is possible, by changing the detector position (from 20° to 70° by 10° steps), to obtain several peaks coming either from $\text{H}(n,p)$, $\text{D}(n,d)$, or $^{12}\text{C}(n,d)^{11}\text{B}$ reactions of 62.7 MeV incident

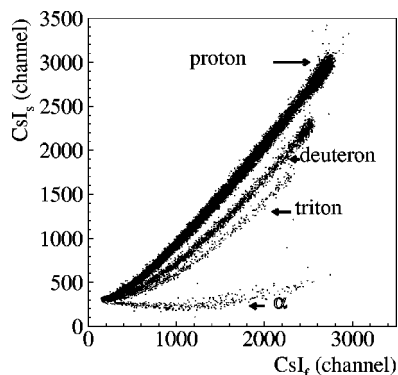
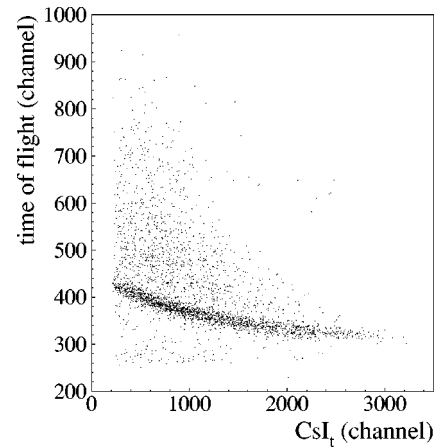


FIG. 4. CsI(Tl) slow versus fast component of the light output.


 FIG. 5. Total time of flight as a function of the measured energy for $^{208}\text{Pb}(n,x\alpha)$ at 20° .

neutrons. These peaks cover a wide energy range from 55.4 MeV at 20° to 7.3 MeV at 70° for proton elastic scattering. The peaks have been corrected to take the energy loss in the target into account. Energy loss corrections are detailed in Sec. III B. For the time calibration, the total time of flight t_{tot} can be calculated using

$$t_{\text{tot}} = t_n + t_{cp}. \quad (1)$$

t_{tot} corresponds to the measured time between the BPO and the ΔE signals. t_n is the time of flight of the neutron from the BPO to the target and is obtained using the neutron flight path ($L=3.28$ m) and its energy ($E_n=62.7$ MeV). t_{cp} is the time of flight of the charged particle from the target to the ΔE detector. It is determined from the particle flight path ($l=31$ cm) and its energy which is known for these reactions.

The energy calibration of the CsI(Tl) for protons (respectively deuterons) is obtained by using elastic scattering on $(\text{C}_3\text{H}_6)_n$ [respectively, $(\text{CD}_2)_n$]. For tritons and α particles, another method based on the correlation between time of flight and the total CsI(Tl) component (CsI_t) has been used. Such a correlation is displayed in Fig. 5 for α particles at 20° for a lead target. A component appears clearly as a line on the figure. It corresponds to the α particles created by 62.7 MeV incident neutrons (which represent 50% of the incident neutrons, see Fig. 2) for which t_n is known. Keeping in mind that the time calibration is already done, it is possible to deduce the α energy from relation (1). The energy calibration has been obtained in that way by selecting several points along this line over the full channel range. The two calibration methods are in good agreement for protons and deuterons giving us confidence in the calibration procedure [4].

Despite the fact that the neutron beam is not monoenergetic, it is possible to deduce, on an event by event basis, the neutrons incident energy. Indeed, for a given event, the charged particle energy and t_{tot} are obtained from the calibration curves and, when injected in Eq. (1), let us determine the neutron energy from its time of flight [4]. It is then possible in one experiment, using 65 MeV protons, to measure

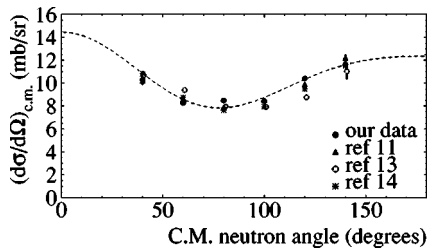


FIG. 6. $H(n,p)$ differential cross sections for 62.7 MeV neutrons in the center of mass. Our data correspond to black dots whereas values obtained by other groups are displayed as triangles [11] and open circles [13]. The stars come from the parametrization of Binstock [14]. The dashed line is the result of a fit using the Legendre polynomials constrained by the Wick limit [15].

cross sections at neutron incident energies ranging from 30 MeV to 62.7 MeV.

The absolute normalization of the lead double differential cross sections was obtained by using the $H(n,p)$ scattering cross section from our $(CH_2)_n$ calibration runs [11]. In Fig. 6, the $H(n,p)$ cross section is displayed as a function of the neutron angle in the center of mass. Black dots correspond to our data whereas results from other groups are presented using other symbols (see figure for details). As can be seen, all these data are in good agreement.

B. Corrections

1. Thick target corrections

The target thickness (0.3 mm for lead) requires that several corrections on the data be made. In order to quantify these corrections, a GEANT [12] simulation of the experimental setup and the beam structure has been done. It allows also to get the solid angle of each detector which is not a trivial task due to our large beam spot and the target orientation.

Particles produced in the lead target can lose a significant amount of their initial energy in the target. This well known effect depends on the charge, the mass and the energy of the emitted particle as well as on the length of crossed material. This affects the entire spectrum. Using GEANT simulations, it is possible to get the correlation between the measured and the emitted energy (true energy) and thus, to correct the spectra for this effect. The energy loss in the target for α particles is much more larger and a simple correction procedure can not be applied in this case. A special procedure is under development inspired by the work of Ref. [16].

A second effect arises from the target thickness but affects only the low energy particles which are created without enough energy to escape the target. Indeed, for these particles, only those created in a fraction of the target, the part close to the output side, can be detected. It is then possible to determine a so-called active target fraction (ATF) which varies between 0 (nothing can escape) and 1 (everything can escape). This number is applied to the counting and depends on the energy and type of the particle emitted. For hydrogen isotopes, the correction starts below the maximum of the coulomb barrier down to 0 and its effect is small due to the relatively low values of the double differential cross section

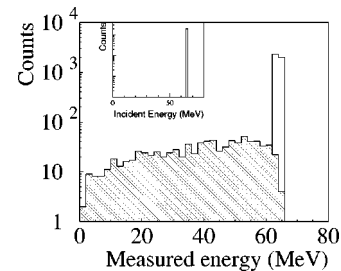


FIG. 7. Simulation showing the effect of proton scattering on the collimators. The inset represents the monoenergetic 65 MeV protons in the lead target (upstream from the collimators) and the spectrum, the response of the CsI(Tl) (downstream from the collimators).

at these energies. For α particles, this effect affects the spectra at energies up to 43 MeV implying a special treatment.

2. Effect of the collimators

The measured spectra also need to be corrected for the scattering of the particles on the telescope collimators. These particles are outside the detection solid angle and are measured over the full energy range. This effect is directly related to the experimental setup and to the quite large beam spot size at the target location [17,18].

To quantify this phenomenon and make corrections, a GEANT simulation has been used based on the following principle: monoenergetic charged particles are created in the target and the response of the CsI(Tl) (downstream from the collimators) is recorded. Figure 7 presents an example of this simulation for monoenergetic 65 MeV protons (see inset) created in the lead target. The energy spectrum of the protons in the CsI(Tl) extends over the complete energy range. Note that the broadening of the peak is due to energy losses in the target. Using the simulation, it is possible to estimate the contribution of the tail, normalized to the peak population, in each energy bin. The iterative correction procedure consists in removing the tail contribution from the spectrum starting from the highest bin: the population of the highest energy bin does not contain any pollution and the corresponding tail contribution can be estimated from the simulation and removed from each lower bin of the spectrum.

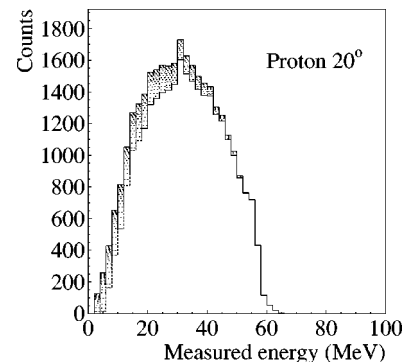


FIG. 8. Proton spectrum before (higher spectrum) and after (lower spectrum) scattering corrections at 20° .

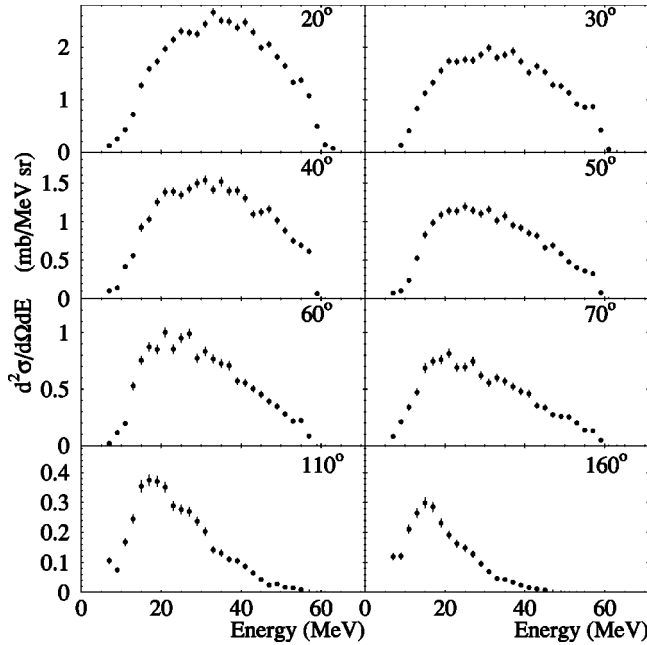


FIG. 9. Double differential cross sections for $^{nat}\text{Pb}(n, xp)$ at 62.7 MeV.

The result of such a procedure is shown in Fig. 8 for protons at 20° in the laboratory. The highest spectrum corresponds to the non-corrected data and the lowest one to the fully corrected data. The effect of the correction increases with decreasing energy due to the accumulation of corrections coming from higher bins. The correction corresponds to an overall effect of 13% for protons, 10% for deuterons, 5% for tritons and is negligible for α particles.

IV. RESULTS

Taking into account all these effects, it is possible to extract precise double differential production cross sections for hydrogen isotopes (see Figs. 9, 10, and 11 for, respectively, the protons, deuterons, and tritons). Energy bins of 2 MeV have been used for protons and deuterons and of 3 MeV for tritons. As stated in the previous section, α particle spectra need special treatment and are not yet available. Only the statistical error is presented in our figures. The systematic error is estimated to about 6%, derived from the measured reference (n, p) cross section (5%), beam monitoring (2%), statistics in the $\text{H}(n, p)$ recoil proton peak (2%), solid angle corrections (1%) and the number of target nuclei (1%).

At 20° , the proton spectrum has a bell-like shape centered around 35 MeV with no sign of direct processes. A comparison of the spectra for different angles, shows that the high energy contribution decreases as the angle increases leading to a Maxwellian-like shape spectrum (at 160°) characteristic of equilibrated source emission. To our surprise, the shape of the spectra shows a strong angular dependence up to 110° . For deuterons and tritons, we observe a high energy peak for forward angles (up to 40°) corresponding to direct processes ($n + \text{Pb} \rightarrow d + \text{Tl}$ for deuteron and $n + \text{Pb} \rightarrow t + \text{Tl}$ for triton). For all hydrogen isotopes, the angular evolution of the spec-

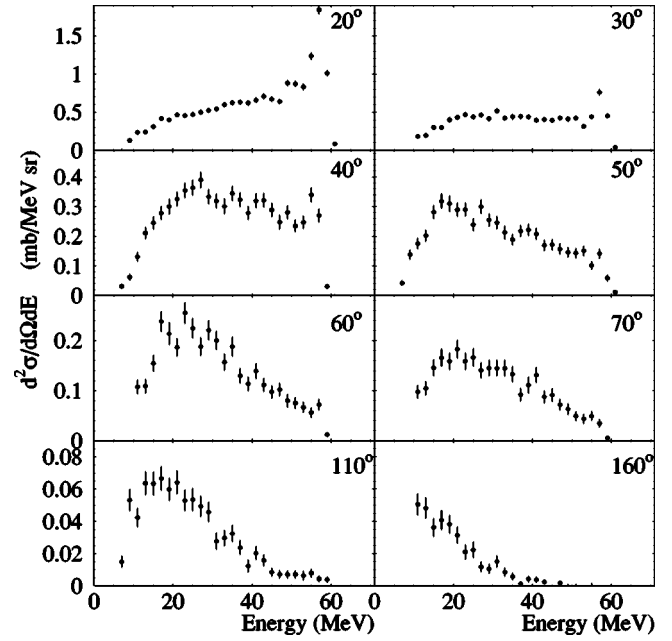


FIG. 10. Double differential cross sections for $^{nat}\text{Pb}(n, xd)$ at 62.7 MeV.

tra shows an anisotropy persisting at backward angles which might be a sign of preequilibrium emission.

From our measurements, it is also possible to extract the experimental angular and the energy differential cross sections. The angular differential cross sections $d\sigma/d\Omega$ are obtained by integrating on the energy range the double differential cross sections. They are displayed in Fig. 12 for protons (open squares), deuterons (triangles), and tritons

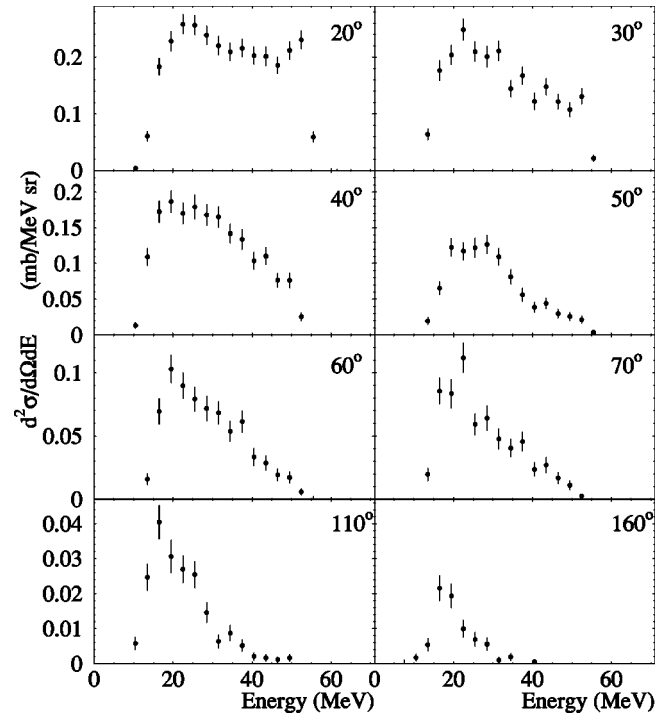


FIG. 11. Double differential cross sections for $^{nat}\text{Pb}(n, xt)$ at 62.7 MeV.

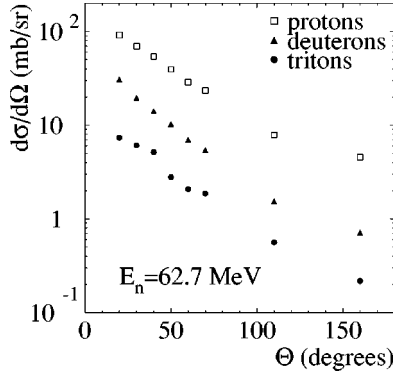


FIG. 12. $d\sigma/d\Omega$ for protons (open squares), deuterons (triangles), and tritons (dots) in $n+Pb$ at 62.7 MeV.

(dots). Spectra are strongly forward peaked for all particles as expected when preequilibrium emission is significant.

The energy differential cross sections are derived directly by fitting our data points using the Kalbach systematics [19,20]. This systematics successfully accounts for a wide variety of experimental angular distributions of proton induced reactions at incident energies up to 200 MeV. It assumes that emitted particles come from either a multistep compound or multistep direct emissions. Within this frame, the angular distribution is expressed as

$$\frac{d^2\sigma}{d\Omega dE} = P_1 \frac{d\sigma}{dE} \frac{P_2}{\sinh(P_2)} \{ \cosh[P_2 \cos(\theta)] + P_3 \sinh[P_2 \cos(\theta)] \},$$

where θ is the emission angle in the center of mass, P_1 , P_2 , and P_3 are the parameters of our fit. P_1 is equal to $1/4\pi$, P_2 corresponds to a slope parameter, and $P_3 = f_{MSD}$, the fraction of the cross section which is assumed to come from multistep direct emission.

The Kalbach systematics does not take into account direct processes and is not efficient in energy regions where these processes are dominant (see, for example, Fig. 10, the high energy part of the deuteron spectra). Figure 13 presents the energy differential cross section $d\sigma/dE$ for the hydrogen isotopes. The symbols have the same meaning as in Fig. 12. The proton spectrum shows a smooth behavior with a maximum around 18 MeV. For the deuteron spectrum, the maximum is

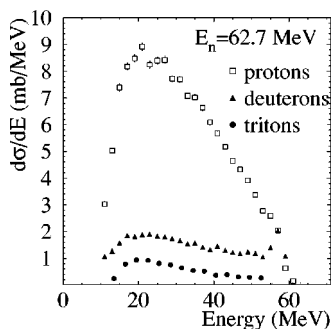


FIG. 13. $d\sigma/dE$ for protons (open squares), deuterons (triangles), and tritons (dots) in $n+Pb$ at 62.7 MeV.

less pronounced and a small rise appears above 53 MeV due to direct processes. For tritons, direct processes appear above 46 MeV.

The production cross sections obtained for the different hydrogen isotopes are reported in the third column of Table I. The first column indicates the particle type whereas the second column the energy range of integration. Indeed, due to the lack of information concerning direct processes (the Kalbach systematics is not fully appropriate and our most forward angle is equal to 20°), we decide to present the experimental integrated cross sections over both the full energy range and with a high energy cut corresponding to the lower limit of the direct processes region.

V. COMPARISON WITH THEORETICAL CALCULATIONS

Comparisons have been done with GNASH-ICRU [22,21,23], TALYS [24], and FLUKA [25] theoretical models which all include a special treatment for preequilibrium processes. The FLUKA code is a Monte Carlo model widely used in high energy experimental physics and engineering, shielding, dosimetry, etc. Each step of this Monte Carlo approach has deep physical basis. The performances are optimized comparing with particle production data at single interaction level. The predictions are obtained with minimal free parameters which are fixed for all energies and target/projectile combinations. It integrates the PEANUT code which is a combination of the intranuclear cascade (INC) and a preequilibrium (exciton [26]) model. This model is the main ingredient for the energy range under consideration in this paper. The INC treatment stops and the statistical pre-equilibrium emission starts when all nucleons have energies below 50 MeV. In this model, secondary nucleons can either escape or reinteract with the nuclei. The decay of an equilibrated nuclei is obtained through a statistical treatment allowing evaporation and/or fission to take place.

The GNASH and TALYS codes integrate the optical model, direct, preequilibrium, fission, and statistical models in one calculation scheme and thereby give a prediction for all the open reaction channels. The GNASH code is widely used in the community to simulate nucleon induced reactions. When secondary emission experimental data exist, certain input parameters are sometimes adjusted within their range of validity to optimize agreement with the measurements. It has to be mentioned that only few data exists for neutron induced reactions in this energy range. GNASH results presented in this paper where obtained and published [23] few years ago before the availability of our data.

TALYS is a new code under development. First, dedicated optical model potentials were developed for both protons and neutrons on ^{208}Pb up to 200 MeV [27]. These potentials provide the necessary reaction cross sections and transmission coefficients for the statistical model calculations. For complex particles, the optical potentials were derived from the nucleon potentials using Watanabe's folding approach [28]. To account for the collective strength at the high-energy part of the neutron spectrum (not shown in this paper), we have included deformation parameters for the first 20 discrete levels of ^{208}Pb and have performed DWBA calcula-

TABLE I. Production cross section obtained in neutron induced reaction on ^{nat}Pb at 62.7 MeV.

Particle type	Energy domain (MeV)	Cross section (mb)	FLUKA (mb)	GNASH/ICRU (mb)		TALYS (mb)
				60 MeV	65 MeV	
proton	full range (≤ 62.7 MeV)	290.0	296.6	442.3	483.5	292.9
deuteron	full range (≤ 62.7 MeV)	75.0		29.80	30.72	87.8
	≤ 53	65.8				
triton	full range (≤ 62.7 MeV)	23.5		3.10	3.14	31.3
	≤ 46	21.6				

tions with ECIS97 [29] to obtain the corresponding direct discrete state cross sections. Collective transitions to the continuum were taken into account by contributions from the giant quadrupole and the low-energy and high-energy octupole resonances. Preequilibrium reactions were modeled with the two-component exciton model of Kalbach [30]. A proton-neutron ratio of 1.6 for the squared internal transition matrix elements was adopted to give the best overall agreement with experiment, i.e., $M_{\pi\pi}^2 = M_{\nu\nu}^2$ and $M_{\pi\nu}^2 = 1.6M_{\nu\nu}^2$. Partial level density parameters $g_{\pi} = Z/13$ and $g_{\nu} = N/13$ were used in the equidistant spacing model. Multiple pre-equilibrium emission is followed up to arbitrary order, though for the incident energy in this experiment only secondary pre-equilibrium emission is significant. The calculated energy spectra were folded with Kalbach's systematics for the angular distribution [20] to obtain the double-differential cross sections. Multiple compound emission was treated with the Hauser-Feshbach model. In this scheme, all reaction chains are followed until all emission channels are closed. We adopted Ignatyuk's model [31] for the total level density to account for the damping of shell effects at high excitation energies. Mass corrections and asymptotical level density and damping parameters were taken from the systematical study of Mengoni and Nakajima [32]. Within this model, the collective enhancement is assumed to be taken into account effectively in the level density parameter. The spectrum calculations were performed for ^{208}Pb . It is worth mentioning that the parameters used to perform the TALYS calculations shown in Fig. 14 also provide similarly good results for (p, xn) and (p, xp) spectra (to be published within the same collaboration).

The results of these three codes have been compared with our data. Let us first focus on global numbers. In Table I, we summarize the production cross section obtained by the codes for the $n + \text{Pb}$ reaction. FLUKA [33] and TALYS results are given for 62.7 MeV incident neutrons energy whereas ICRU data which are the only published results [22] are available only at 60 or 65 MeV. So in order to make meaningful comparisons, we provide ICRU results at both energies. The experimental values appear in the third column. ICRU results overestimate proton production by a large amount. On the other hand, it strongly underestimates the deuteron and triton values. Both FLUKA and TALYS are in good agreement with our results for the proton production cross section. TALYS is also able to give emission spectra of composite particles. In our case, the deuteron and triton pro-

duction cross sections calculated by TALYS are in agreement with the data (see Table I). Since FLUKA has not provided values for composite particles, we will focus on (n, xp) reactions for FLUKA and TALYS.

In Fig. 14, the double differential cross sections for protons are reported at four different angles (20° , 40° , 60° , and 160°). Theoretical results are presented as lines. The right hand column shows TALYS data (full lines) whereas FLUKA data (dashed lines) are plotted in the left hand column. In all these plots, the black dots correspond to our data. In both calculations the shapes of the spectra are in close agreement with the data. They both underestimate the pre-equilibrium component around 30 MeV at 20° . In addition, FLUKA overestimates the thermal emission at backward angles. Nevertheless, both give a good estimation of the proton production cross section.

VI. CONCLUSION

Proton, deuteron, and triton double differential production cross sections have been measured in 62.7 MeV neutron-

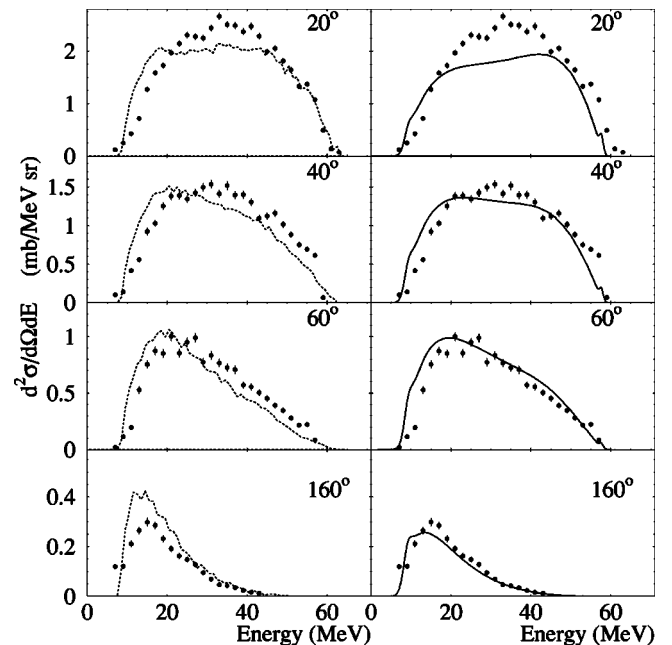


FIG. 14. Proton for $n + \text{Pb}$ at 62.7 MeV. Dots are the experimental data whereas dashed (full) line in the left hand (right hand) column corresponds to FLUKA (TALYS) results.

induced reactions on a natural lead target. Special attention has been devoted to the correction procedures which are necessary because we use thick target and collimators. Measurements were done with good statistics. The comparison with some well-known theoretical code results was performed. GNASH-ICRU data shows a large difference on the production cross section values for hydrogen isotopes. TALYS and FLUKA give a good estimation of the proton cross-section value. Other data on lead using proton-induced reactions at the same beam energy are being analyzed and will be published soon to enrich the data tables [6].

ACKNOWLEDGMENTS

This work was supported partly by the European Community under Contract No. FIKW-CT-2000-0031 and under the concerted action NoFI4I-CT98-0017 and by the GDR GEDEON (research group CEA - CNRS - EDF - FRAM-ATOME). We would like to thank the Louvain-la-Neuve cyclotron staff for permanent assistance and quality of the beam. We acknowledge also, the Institut Interuniversitaire des Sciences Nucléaires, Belgium, for its financial support of this experiment.

-
- [1] C.D. Bowman *et al.*, Nucl. Instrum. Methods Phys. Res. A **320**, 336 (1992).
- [2] C. Rubbia *et al.*, Report No. CERN/AT95-44(ET), 1995.
- [3] J. Cugnon, C. Volant, and S. Vuillier, Nucl. Phys. **A620**, 475 (1997).
- [4] M. Kerveno, Ph.D. thesis, Nantes University, 2000.
- [5] A.J. Koning, J.P. Delaroche, and O. Bersillon, Nucl. Instrum. Methods Phys. Res. A **414**, 49 (1998).
- [6] HINDAS: High and Intermediate energy Nuclear Data for Accelerator-driven Systems, European community, Contract No. FIKW-CT-2000-0031.
- [7] A. Bol, P. Leleux, P. Lipnik, P. Macq, and A. Ninane, Nucl. Instrum. Methods **214**, 169 (1983).
- [8] I. Slypen, V. Corcalciuc, and J.P. Meulders, Nucl. Instrum. Methods Phys. Res. B **88**, 275 (1994).
- [9] I. Slypen, V. Corcalciuc, and J.P. Meulders, Phys. Rev. C **51**, 1303 (1995).
- [10] I. Slypen, V. Corcalciuc, A. Ninane, and J.P. Meulders, Nucl. Instrum. Methods Phys. Res. A **337**, 431 (1997).
- [11] S. Benck, I. Slypen, V. Corcalciuc, and J.P. Meulders, Eur. Phys. J. A **3**, 149 (1998).
- [12] GEANT: CERN program library long write-up W5013
- [13] N.S.P. King, J.D. Reber, J.L. Romero, D.H. Fitzgerald, J.L. Ullmann, T.S. Subramanian, and F.P. Brady, Phys. Rev. C **21**, 1185 (1980).
- [14] J. Binstock, Phys. Rev. C **10**, 19 (1974).
- [15] P.E. Hodgson, *Nuclear Reaction and Nuclear Structure* (Clarendon, Oxford, 1971), p. 91.
- [16] P.S. Rezentes, J.L. Romero, and C.M. Castaneda, Nucl. Instrum. Methods Phys. Res. A **361**, 574 (1995).
- [17] A.A. Cowley, C.C. Chang, and H.D. Holmgren, Phys. Rev. C **22**, 2633 (1980).
- [18] F.E. Bertrand, W.R. Burrust, N.W. Hill, T.A. Love, and R.W. Peelle, Nucl. Instrum. Methods Phys. Res. A **101**, 475 (1972).
- [19] C. Kalbach and F.M. Mann, Phys. Rev. C **23**, 112 (1981); C. Kalbach, *ibid.* **23**, 124 (1981).
- [20] C. Kalbach, Phys. Rev. C **37**, 2350 (1988).
- [21] P.G. Young, E.D. Arthur, and M.B. Chadwick, Report No. LA-12343-MS, 1992.
- [22] International Commission on Radiation Units and Measurements, Report No. 63, 1999.
- [23] M.B. Chadwick, P.G. Young, S. Chiba, S.C. Frankle, M. Hale, H.G. Hughes, A.J. Koning, R.C. Little, R.E. Macfarlane, R.E. Prael, and L.S. Waters, Nucl. Sci. Eng. **131**, 293 (1999).
- [24] A.J. Koning and S. Hilaire (unpublished); A.J. Koning *et al.*, Proceedings of the INDC 2001, Tsukuba, Japan, 2001 (unpublished).
- [25] A. Ferrari and P.R. Sala, *Proceedings of the MC93 International Conference on Monte Carlo Simulation in High Energy and Nuclear Physics*, Tallahassee, Florida, 1993 (World Scientific, Singapore, 1993), p. 277.
- [26] M. Blann and H. K. Vonach, Phys. Rev. C **28**, 1475 (1983).
- [27] A.J. Koning and J.P. Delaroche (unpublished).
- [28] S. Watanabe, Nucl. Phys. **8**, 484 (1958).
- [29] J. Raynal, Notes on ECIS94, CEA Saclay Report No. CEA-N-2772, 1994.
- [30] C. Kalbach, Phys. Rev. C **33**, 818 (1986).
- [31] A.V. Ignatyuk, G.N. Smirenkin, and A.S. Tishin, Sov. J. Nucl. Phys. **21**, 255 (1975).
- [32] A. Mengoni and Y. Nakajima, J. Neurosci. Methods **31**, 151 (1994).
- [33] These calculations on natural lead have been performed in Nantes by Yann Foucher.